Physics of Fluids

Thermocapillary instabilities in a liquid layer subjected to an oblique temperature gradient: Effect of a prescribed normal temperature gradient at the substrate

Cite as: Phys. Fluids **32**, 112109 (2020); https://doi.org/10.1063/5.0029477
Submitted: 13 September 2020 . Accepted: 30 October 2020 . Published Online: 17 November 2020

Ramkarn Patne, Yehuda Agnon, and Alexander Oron

Physics of Fluids ARTICLE scitation.org/journal/phf

Thermocapillary instabilities in a liquid layer subjected to an oblique temperature gradient: Effect of a prescribed normal temperature gradient at the substrate

Cite as: Phys. Fluids 32, 112109 (2020); doi: 10.1063/5.0029477
Submitted: 13 September 2020 • Accepted: 30 October 2020 •
Published Online: 17 November 2020

Ramkarn Patne,[1,2] Yehuda Agnon,[1] and Alexander Oron[2,a)]

AFFILIATIONS

[1] Faculty of Civil and Environmental Engineering, Technion-Israel Institute of Technology, Haifa 3200003, Israel
[2] Faculty of Mechanical Engineering, Technion-Israel Institute of Technology, Haifa 3200003, Israel

[a)] **Author to whom correspondence should be addressed:** meroron@technion.ac.il

ABSTRACT

We consider thermocapillary instability in a three-dimensional liquid layer with a deformable interface with an ambient gas phase and subjected to an oblique temperature gradient when the temperature gradient at the substrate is prescribed. We demonstrate that this configuration leads to a drastic change in the instability features with respect to those emerging when either a purely vertical temperature gradient (VTG) or a purely horizontal temperature gradient (HTG) is present. In the case of the return flow as the base state, the spanwise long-wave instability mode dominates except for the range of small Bond numbers *Bo*. Slippage at the substrate has a stabilizing (destabilizing) effect on streamwise (spanwise) long-wave modes in the presence of a HTG. In the case of linear flow as the base state, both streamwise and spanwise long-wave modes play a major role in the instability onset depending on the ratio between the HTG and the VTG η for higher values of the capillary number *Ca*, e.g., $Ca > 0.001$. However, for lower values of *Ca*, e.g., $Ca < 0.001$, streamwise and spanwise instability modes become finite-waves at large η. In contrast to the return flow, for the linear flow, slippage at the substrate destabilizes both long-wave modes.

I. INTRODUCTION

Thermocapillary instability arising from surface-tension inhomogeneity at the free interface of a liquid layer deposited on a planar solid wall and subjected to a purely vertical temperature gradient (VTG) was first theoretically studied by Pearson[1] in the case of the flat interface. He showed the emergence of thermocapillary instability as a consequence of surface-tension dependence on the temperature at the layer interface. His results were extended[2–5] to liquid layers with a deformable surface, i.e., the liquid–gas interface with a finite surface tension. This analysis revealed a strong effect of a decrease in surface tension on the instability, which is due to a stronger temperature variation along the interface. Thermocapillary instabilities originating from temperature dependence of the surface tension are frequently encountered in microfluidics applications,[6] additive manufacturing,[7] material processing and crystal growth,[8] and also various industrial processes such as coating and drying.[9]

Thermocapillary instabilities in a liquid layer subjected to a purely horizontal temperature gradient (HTG) were studied first by Smith and Davis[10,11] and in subsequent studies.[7,12–14] Instabilities investigated by Smith and Davis[10,11] were experimentally observed in Refs. 15–20. Reviews on the subject of thermocapillary instabilities can be found in Refs. 21 and 18.

In various applications and experiments, however, liquid layers are exposed, intentionally due to the process design[22,23] or unintentionally due to practical imperfections, to an oblique temperature gradient (OTG) instead of either a purely VTG or a purely HTG. Thus, an understanding of thermocapillary instabilities exhibited by a liquid layer subjected to an OTG becomes an inevitable

necessity to avoid undesirable dynamics and patterns. Nepomnyashchy *et al.*[22–25] and Patne *et al.*[26] studied the stability of a liquid layer subjected to an OTG. These studies revealed a strong stabilizing effect of the HTG on instabilities triggered by a purely VTG. Patne *et al.*[26] recently showed that in the case of a constant temperature difference across the layer, the stabilizing effect of the HTG arises due to an additional VTG component *induced* by the HTG, which counteracts the imposed VTG, leading thereby to a revealed stabilization. Furthermore, an interaction between the VTG and the HTG leads to the emergence of a new unstable mode, which becomes the dominant mode of instability even when the strength of the HTG is higher than that of the VTG.

Previous studies[22–24,26] on thermocapillary instabilities in a liquid layer subjected to an OTG assumed a constant temperature difference between the substrate and the ambient gas phase across the layer. However, in numerous technological processes, the normal temperature gradient at the substrate is preferred due to the ease of operation or arises out of the physics of the problem. In addition, in the case of a solid substrate of thermal conductivity lower than that of the liquid, the boundary condition of an imposed normal temperature gradient at the substrate becomes more appropriate than that of a prescribed temperature.[27] The change in the thermal boundary condition at the substrate leads to a drastic change in thermocapillary instabilities exhibited by the system. Furthermore, as shown in Secs. II, IV, and VI, the HTG interacts in a completely different way with the VTG when compared with the case of a constant temperature difference across the layer studied in previous papers.[22–24,26]

The rest of this paper is arranged as follows: The problem statement, the original governing equations and boundary conditions, the base-state fields, and the governing equations for the perturbations are presented in Sec. II. The pseudospectral numerical approach used in the solution of the linear eigenvalue problem obtained in the context of the general linear stability analysis (GLSA) is outlined in Sec. III. The results of the GLSA are presented in Sec. IV. The asymptotic analysis for the long-wave mode is carried out in Sec. V. The major conclusions of the present study are summarized in Sec. VI.

II. PROBLEM FORMULATION

We consider a three-dimensional horizontal layer of an incompressible Newtonian liquid with temperature-independent properties such as dynamic viscosity μ, density ρ, kinematic viscosity ν, and thermal diffusivity κ deposited on a horizontal planar substrate in the gravity field g schematically shown in Fig. 1. The layer is assumed to be of mean thickness d and have an infinite lateral extent. The liquid layer is bounded by the ambient inert gas phase at the liquid–gas interface, which is assumed to be deformable.

The coordinate system used here is Cartesian with the axes x^* and z^* located in the substrate plane, whereas the axis y^* is normal to the substrate and directed into the liquid layer with the reference point $y^* = 0$ located on the substrate plane. In what follows, the asterisk denotes dimensional variables, whereas their dimensionless counterparts are denoted by the same letters without an asterisk.

The entire system consisting of the substrate, the liquid layer, and the gas phase is subjected to an oblique temperature gradient with the constant horizontal (HTG) and vertical (VTG) components

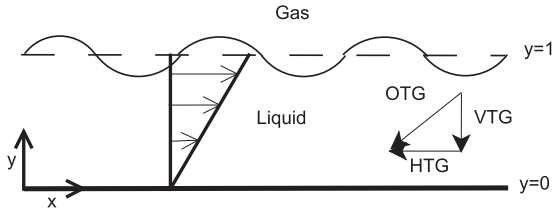

FIG. 1. Sketch of the system considered here. A liquid layer supported by a substrate at $y = 0$ is subjected to an OTG with the VTG component $-\beta^*$ and the HTG component $-\eta^*$, each shown by an arrow. The HTG induces a thermocapillary flow shown by the linear velocity profile. If the side walls are present in the x-direction, then the HTG leads to the emergence of the return flow and the velocity profile changes. The waves shown at the gas–liquid interface illustrate interfacial perturbations.

$-\eta^*$ and $-\beta^*$, respectively. The layer is assumed to be sufficiently thin, so the buoyancy effect could be neglected.

Surface tension at the liquid–gas interface σ^* is assumed to vary linearly with the temperature

$$\sigma^* = \sigma_0^* - \gamma^*(T^* - T_0^*), \tag{1}$$

where $\gamma^* = -d\sigma^*/dT^* > 0$ and σ_0^* is the reference surface tension of the fluid at the reference temperature, for instance, that related to the lower plate taken as T_0^*. This variation of surface tension along the liquid–gas interface generates Marangoni shear stresses, which may be liable for the onset of instability of the base state of the system. The present study assumes a linear dependence of the interfacial tension on the temperature. Thermocapillary instabilities in a liquid layer with a nonlinear relationship between the surface tension and the temperature subjected to a VTG were studied by Oron and Rosenau,[28] Batson *et al.*,[29] and Sarma and Mondal.[30]

A liquid layer subjected to an OTG can exhibit two types of flows. One of them is a linear flow where the presence of side boundaries is neglected, yielding thereby a linear velocity profile.[10,11] A schematic of the linear flow that may be encountered in industrial processes[7] is shown in Fig. 1. The other one is the return flow, which arises if the presence of the side boundaries is not neglected and is taken into account. It may arise in industrial processes or experiments where thermocapillary instabilities are studied in cavities.[10,11] The forthcoming analysis considers both types of flows.

The length, time, velocities, and temperature gauged against T_∞ are nondimensionalized by d, d^2/κ, κ/d, and $\beta^* d$, respectively, and pressure and stresses are nondimensionalized by $\mu\kappa/d^2$. We denote the dimensionless fluid velocity field as $\mathbf{v} = (v_x, v_y, v_z)$, with v_i being the respective velocity components in the direction $i = x, y, z$. The dimensionless continuity and momentum conservation equations are

$$\nabla \cdot \mathbf{v} = 0, \tag{2a}$$

$$\frac{1}{Pr}[\partial_t \mathbf{v} + (\mathbf{v} \cdot \nabla)\mathbf{v}] = -\nabla p - GPr\nabla y + \nabla^2 \mathbf{v}, \tag{2b}$$

where $Pr = \mu/\rho\kappa$ is the Prandtl number, $G = gd^3/\nu^2$ is the Galileo number, $\nabla = (\partial_x, \partial_y, \partial_z)$ is the gradient operator, $\nabla^2 \equiv \partial_x^2 + \partial_y^2 + \partial_z^2$ is the Laplacian operator, p is the pressure, and $\partial_\times$ denotes the partial derivative with respect to $\times$. The dimensionless heat advection–diffusion equation is

$$\partial_t T + (\mathbf{v}\cdot\nabla)\, T = \nabla^2 T. \tag{2c}$$

When a liquid layer is deposited on a rough-walled hydrophobic surface,[31] a slip of the liquid at the substrate is possible in general, and in thermocapillary flows promoted by an imposed HTG, in particular. In the additive manufacturing process, to model the dynamics of a fluid system, a slip at the substrate is essential,[7] and the present analysis assumes the existence of slippage.

The governing equations (2) are subjected to the following dimensionless boundary conditions: Navier slip, impermeability, and a constant specified normal temperature gradient at the solid substrate $y = 0$, yielding

$$v_x = \zeta\partial_y v_x; \quad v_y = 0; \quad v_z = \zeta\partial_y v_z; \quad \partial_y T = -1, \tag{3a}$$

where ζ is the dimensionless Navier slip parameter.

At the deformable gas–liquid interface located at $y = 1 + \xi(x, y, t)$, where $\xi(x, z, t)$ is the infinitesimal displacement of the interface from its undisturbed position $y = 1$, the boundary conditions are the kinematic boundary condition, the tangential and normal components of the stress balance,[5] and the continuity of the heat flux, respectively,

$$\partial_t \xi + \mathbf{v}_\perp \cdot \nabla\xi = v_y, \tag{3b}$$

$$\mathbf{t}_j \cdot \boldsymbol{\tau} \cdot \mathbf{n} = -Ma\nabla T \cdot \mathbf{t}_j, \tag{3c}$$

$$-p + \mathbf{n}\cdot\boldsymbol{\tau}\cdot\mathbf{n} = -Ca^{-1}(\nabla\cdot\mathbf{n}) - Bo\, Ca^{-1}\xi, \tag{3d}$$

$$\nabla T \cdot \mathbf{n} = -Bi(T + \eta x), \tag{3e}$$

where

$$Ma = \frac{\gamma\beta^* d^2}{\mu\kappa}, Bo = \frac{\rho g d^2}{\sigma_0^*}, Bi = \frac{qd}{k_{th}}, Ca = \frac{\mu\kappa}{\sigma_0^* d}, \eta = \frac{\eta^*}{\beta^*} \tag{4}$$

are, respectively, the Marangoni, Bond, Biot, and capillary numbers and the dimensionless HTG, with $Bo = GCaPr$ and $j = 1, 2$. Here, q, σ_0^*, g, and k_{th} are the coefficient of thermal convection at the free surface, surface tension evaluated at the temperature at some location along the free surface, gravity acceleration, and the thermal conductivity of the fluid. The vectors $\mathbf{t}_j$ and $\mathbf{n}$ represent the unit tangent and normal vectors to the free surface, respectively. In addition, $\boldsymbol{\tau}$ is the deviatoric stress tensor with the components $\tau_{ij} = \frac{1}{2}(\partial_j v_i + \partial_i v_j)$, $(v_x, v_y, v_z) \equiv (v_1, v_2, v_3)$, and $(x, y, z) \equiv (x_1, x_2, x_3)$, and the vector $\mathbf{v}_\perp$ is the two-dimensional vector obtained by projection of $\mathbf{v}$ onto the x–z plane, $\mathbf{v}_\perp = (v_x, v_z)$.

The linearized (without taking into consideration the interfacial metrics) expressions for the normal $\mathbf{n}$ and tangential $\mathbf{t_1}$ and $\mathbf{t_2}$ vectors at the free surface in the perturbed state are given by

$$\mathbf{n} = -\partial_x\xi\,\mathbf{e_x} + \mathbf{e_y} - \partial_z\xi\,\mathbf{e_z}, \quad \mathbf{t}_1 = \mathbf{e_x} + \partial_x\xi\,\mathbf{e_y}, \quad \mathbf{t}_2 = \partial_z\xi\,\mathbf{e_y} + \mathbf{e_z}. \tag{5}$$

The vectors $\mathbf{e_x}$, $\mathbf{e_y}$, and $\mathbf{e_z}$ are the unit vectors in the x-direction, y-direction, and z-direction, respectively.

A. Base state

A liquid layer subjected to an OTG can exhibit two types of flows. One of them is a linear flow for which the presence of the side boundaries is neglected, thereby yielding a linear velocity profile.[10,11] Such a flow could be encountered in geophysical systems or industrial processes.[7] The other one is the return flow, which arises if the presence of the side boundaries is taken into account. The return flow can arise in the industrial processes or during the experiments to study thermocapillary instabilities[10,11] in cavities.

For the base state, the properties are denoted with a double overbar; the governing equations (2) are subjected to the boundary conditions of Navier slip, impermeability, and a constant normal temperature gradient at the solid substrate $y = 0$, which are

$$\overline{\overline{v}}_x = \zeta\partial_y\overline{\overline{v}}_x. \quad \overline{\overline{v}}_y = 0, \quad \overline{\overline{v}}_z = \zeta\partial_y\overline{\overline{v}}_z, \quad \partial_y\overline{\overline{T}} = -1. \tag{6a}$$

At the undisturbed gas–liquid interface $y = 1$, the boundary conditions are the kinematic boundary condition, the tangential component of the stress balance, and the continuity of the heat flux, respectively,

$$\overline{\overline{v}}_y = 0, \qquad \partial_y\overline{\overline{v}}_x = -Ma\partial_x\overline{\overline{T}}, \qquad \partial_y\overline{\overline{T}} = -Bi(\overline{\overline{T}} + \eta x). \tag{6b}$$

For the return flow, there will be an additional boundary condition implying a zero total volumetric flow rate,

$$\int_0^1 \overline{\overline{v}}_x dy = 0. \tag{6c}$$

The governing equations (2) and boundary conditions (6) determine the base state for the linear flow in the form

$$\overline{\overline{v}}_x = \eta\, Ma\,(y + \zeta), \quad \overline{\overline{v}}_y = 0, \quad \overline{\overline{v}}_z = 0, \quad \overline{\overline{p}} = p_a - G\,Pr\,y, \tag{7a}$$

$$\overline{\overline{T}}(x, y) = C_1 - \eta x - y - \frac{1}{2}\zeta\eta^2 May^2 - \frac{1}{6}\eta^2 May^3, \tag{7b}$$

where C_1 is an integration constant. A comparison of the base-state temperature for the fixed temperature difference across the layer given by Patne *et al.*[26] with the base-state temperature for a fixed temperature gradient at the substrate given by Eq. (7b) reveals that the HTG induces an additional linear VTG in the former case, whereas in the latter case, it does not.

Similarly, the base state for the return flow is

$$\overline{\overline{v}}_x = \frac{\eta Ma\left[y(-2 + 3y) + \zeta(-2 + 6y^2)\right]}{4(1 + 3\zeta)}, \quad \overline{\overline{v}}_y = 0, \quad \overline{\overline{v}}_z = 0, \quad \overline{\overline{p}} = p_a - G\,Pr\,y, \tag{8a}$$

$$\overline{\overline{T}}(x, y) = C_2 - \eta x - y - \frac{\eta^2\, Ma}{4(1 + 3\zeta)}\left(-\zeta y^2 - \frac{y^3}{3} + \frac{(1 + 2\zeta)y^4}{4}\right), \tag{8b}$$

where C_2 is an integration constant. The exact values of the constants C_1 in Eq. (7b) and C_2 in Eq. (8b) are immaterial for the further analysis to be carried out below.

B. Perturbed state

Next, infinitesimal perturbations are imposed on each of the base states [Eqs. (7) and (8)] to carry out the linear stability analysis

of the respective base states of the system. Squire's theorem[32] is not applicable in the present case due to the imposed HTG; thus in what follows, three-dimensional disturbances are considered. The governing equations are then linearized around the base states [Eqs. (7) and (8)], and normal modes,

$$f'(\mathbf{x},t) = \tilde{f}(y)\exp(ikx + imz + st),$$
$$\xi(x,z,t) = \tilde{\xi}\exp(ikx + imz + st), \tag{9}$$

are substituted into these. Here, $f'(\mathbf{x}, t)$ is a perturbation to a dynamic quantity $f(\mathbf{x}, t)$, such as the components of the fluid velocity field v_x, v_y, and v_z, pressure p, and temperature T, $\tilde{f}(y)$ is the corresponding eigenfunction in the Laplace–Fourier space, and $\tilde{\xi}$ is a constant. The parameters k and m are the wavenumbers of the perturbations in the x-direction and z-direction, respectively, and the value $s = s_r + is_i$ is the complex growth rate. The base-state flow is linearly unstable if at least one eigenvalue of the resulting problem satisfies the condition $s_r > 0$. This procedure leads to the linearized continuity, momentum conservation, and energy equations, which read as

$$ik\tilde{v}_x + D\tilde{v}_y + im\tilde{v}_z = 0, \tag{10a}$$

$$\frac{1}{Pr}\left[s\tilde{v}_x + ik\overline{\overline{v}}_x\tilde{v}_x + \tilde{v}_y D\overline{\overline{v}}_x\right] = -ik\tilde{p} + (D^2 - k^2 - m^2)\tilde{v}_x, \tag{10b}$$

$$\frac{1}{Pr}\left[s\tilde{v}_y + ik\overline{\overline{v}}_x\tilde{v}_y\right] = -D\tilde{p} + (D^2 - k^2 - m^2)\tilde{v}_y, \tag{10c}$$

$$\frac{1}{Pr}\left[s\tilde{v}_z + ik\overline{\overline{v}}_x\tilde{v}_z\right] = -im\tilde{p} + (D^2 - k^2 - m^2)\tilde{v}_z, \tag{10d}$$

$$s\tilde{T} + ik\overline{\overline{v}}_x\tilde{T} + \partial_x\overline{\overline{T}}\,\tilde{v}_x + \partial_y\overline{\overline{T}}\,\tilde{v}_y = (D^2 - k^2 - m^2)\tilde{T}, \tag{10e}$$

where $D \equiv d/dy$. Equations (10) are then supplemented with the boundary conditions

$$y = 0: \quad \tilde{v}_x = \zeta D\tilde{v}_x, \quad \tilde{v}_y = 0, \quad \tilde{v}_z = \zeta D\tilde{v}_z, \quad D\tilde{T} = 0. \tag{11a}$$

At the deformable boundary, following the standard procedure of projection of the boundary conditions at the deformed interface $y = 1 + \xi$ onto $y = 1$, the boundary conditions at $y = 1$ read as

$$\tilde{v}_y = s\tilde{\xi} + ik\overline{\overline{v}}_x\tilde{\xi}, \tag{11b}$$

$$\tilde{\tau}_{xy} + \tilde{\xi}\,D^2\overline{\overline{v}}_x = -ik\,Ma\left(\tilde{T} + \tilde{\xi}\,\partial_y\overline{\overline{T}}\right), \tag{11c}$$

$$\tilde{\tau}_{yz} = -im\,Ma\left(\tilde{T} + \tilde{\xi}\,\partial_y\overline{\overline{T}}\right), \tag{11d}$$

$$-\tilde{p} + \tilde{\tau}_{yy} - 2ik\tilde{\xi}\,D\overline{\overline{v}}_x = -\frac{(Bo + k^2 + m^2)}{Ca}\tilde{\xi}, \tag{11e}$$

$$D\tilde{T} + Bi\tilde{T} + \left(-ik\partial_x\overline{\overline{T}} + \partial_y^2\overline{\overline{T}} + Bi\partial_y\overline{\overline{T}}\right)\tilde{\xi} = 0. \tag{11f}$$

While deriving the normal stress balance boundary condition (11e), it has been assumed that the thermocapillary contribution to the normal stress balance is negligible, i.e.,

$$\gamma^*\left(\overline{\overline{T}}^*|_{y^*=d} - T_0^*\right)/\sigma_0^* = Ma\,Ca\left(\overline{\overline{T}}|_{y=1} - T_0\right) \ll 1. \tag{12}$$

Since for most of liquids $Ma\,Ca \ll 1$ at the onset of linear instability, this assumption holds true provided that $(\overline{\overline{T}}|_{y=1} - T_0) = O(1)$. This also helps to proceed with the normal mode analysis by removing the term $\overline{\overline{T}}|_{y=1}$, which depends on x and therefore could represent an obstacle.

Equations (10) and (11) constitute a generalized linear eigenvalue problem, which is to be solved in terms of the eigenvalues s and the eigenfunctions for a specified set of parameter values Bi, Bo, Ca, Pr, and Ma. To determine the spectrum of the eigenvalue problem (10) and (11), the pseudospectral method is employed, details of which are presented below.

III. NUMERICAL APPROACH

To carry out the linear stability analysis of the problem at hand, the pseudospectral method is employed in which the eigenfunctions corresponding to each dynamic field are expanded into a series of Chebyshev polynomials as

$$\tilde{f}(y) = \sum_{m=0}^{m=N} a_m T_m(y), \tag{13}$$

where $T_m(y)$ are Chebyshev polynomials of degree m and N is the highest degree of the polynomial in the series expansion or, equivalently, the number of collocation points. The series coefficients a_m are the unknowns to be solved for.

For convenience, the domain $0 \le y \le 1$ is transformed into $-1 \le y \le 1$ by stretching mapping $y \to 2y - 1$. The generalized eigenvalue problem is finally obtained in the form

$$\mathbf{Ae} + s\mathbf{Be} = 0, \tag{14}$$

where $\mathbf{A}$ and $\mathbf{B}$ are matrices derived following the discretization procedure and $\mathbf{e}$ is the vector containing the coefficients of all series expansions (A1).

Further details of the discretization of the governing equations and boundary conditions and of the construction of the matrices $\mathbf{A}$ and $\mathbf{B}$ can be found in the standard procedure described by Trefethen[33] and Schmid and Henningson.[32] The application of the pseudospectral method for similar problems can be found in Patne *et al.*[26,34] We use the *polyeig* MATLAB routine to solve the constructed generalized eigenvalue problem given by Eq. (14). To filter out the spurious modes from the genuine numerically computed spectrum of the problem, the latter is obtained for N and $N + 2$ collocation points, and the eigenvalues are compared with a specified tolerance, e.g., 10^{-4}. The genuine eigenvalues are verified by increasing the number of collocation points by 25 and monitoring the variation of the obtained eigenvalues. Whenever the eigenvalue does not change more than a specified precision, e.g., to the sixth significant digit, the same number of collocation points is used to determine the critical parameters of the system. In the present work, $N = 75$ is found to be sufficient to achieve convergence and to determine the leading, most unstable eigenvalue within the investigated parameter range.

IV. RESULTS AND DISCUSSION

For the ease of the presentation of the results and their discussion, the contents of this section have been split into Sec. IV A

dedicated to the return flow and Sec. IV B to the linear flow. The ranges for the dimensional parameters are $d \sim 10^{-6}$–10^{-3} m, $\rho \sim 10^3$ kg/m^3, $\gamma \sim 10^{-5} \sim 10^{-3}$ N m/K, $k_{th} \sim 10^{-6}$–10^{-3} J/(m s K), $q \sim 1$–10^2 J/(m^2 s K), $\kappa \sim 10^{-7}$–10^{-5} m^2/s, $\mu \sim 10^{-3}$–10^2 Pa s, and $\sigma_0^* \sim 10^{-3} - 10^{-1}$ N/m.[19,35–37] Accordingly, the corresponding dimensionless numbers are $Bi \sim O(10^{-3}$–$10)$, $Bo \sim O(10^{-3}$–$10^{-1})$, $Ca \sim O(10^{-6}$–$10^{-1})$, and $Pr \sim O(1$–$10^3)$. To describe technological processes such as additive manufacturing, fluid-flow models require accounting for slippage with the slip parameter[7] $\zeta \sim O(10)$. In other cases such as flows past hydrophobic and grooved surfaces,[38] ζ ranges from 0.001 to 0.1. This parameter range will be used in the present study to analyze various modes of instability.

A. Return flow

The stability of the return flow subjected to a purely HTG was first studied by Smith and Davis.[10,11] Their analysis indicated the absence of the stationary rolls unlike in the case of the linear flow. However, oblique hydrothermal waves were predicted in their study for the return flow.

A liquid layer with a deformable surface subjected to a purely VTG exhibits a long-wave mode of instability either due to the constant temperature gradient at the substrate[1] or due to the deformability of the free surface.[5] If an OTG is imposed, then the linear or return flow will affect the long-wave instability, as shown in Fig. 2.

Figure 2 shows that an increase in η, i.e., in the strength of the imposed HTG component, has a destabilizing effect on both streamwise and spanwise long-wave modes. Furthermore, for a nonzero η, the streamwise long-wave mode becomes an upstream traveling mode. It must be stressed that for the linear flow irrespective of the boundary condition at the substrate, the imposed HTG, as shown below, makes the stationary streamwise mode a downstream traveling mode.[26]

In the case of a constant imposed temperature difference across the layer of Patne *et al.*,[26] the imposed HTG component induces a VTG counteracting the imposed VTG component, which leads to the stabilization of the streamwise long-wave mode originated from the deformability of the free surface. However, the lack of the opposing VTG induced by the imposed HTG in the present problem leads to the absence of the stabilization of the long-wave instability. As shown in Fig. 2(b), the imposed HTG also destabilizes the spanwise long-wave mode, but in contrast to the streamwise long-wave mode, it remains stationary, $s_i = 0$.

The variation of the critical Marangoni number Ma_c for the streamwise and spanwise long-wave modes is shown in Fig. 3 for two representative values of the capillary number. Irrespective of the value of the capillary number, the curves, if extended into the range of large η, scale as $Ma_c \sim 1/\eta$. For $Ca = 0.01$, as shown in Fig. 3(a), the spanwise long-wave mode possesses a lower Ma_c as compared to the streamwise long-wave mode. Thus, the spanwise long-wave mode represents the dominant mode of instability. The curves for $Ca = 0.0001$, as displayed in Fig. 3(b), show that an increase in the HTG has a stabilizing effect on the streamwise long-wave mode. However, an increase in the HTG has a destabilizing effect on the spanwise long-wave mode. Thus, to enable the emergence of the streamwise mode in the domain of higher values of η, a sufficiently large value of the capillary number is necessary. It is important to note that a liquid layer subjected to a purely HTG does not exhibit a long-wave thermocapillary instability[11] revealed here. However, even at high η, we observe that the liquid layer not only supports the long-wave thermocapillary instability but also represents the dominant mode of instability. In addition, with a low capillary number, the streamwise long-wave instability is confined to an island similar to that was found in the case of an imposed constant temperature across the layer.[26]

Figure 4 shows the effect of variation in the Biot number Bi in panel (a) and in the Bond number Bo in panel (b) on the

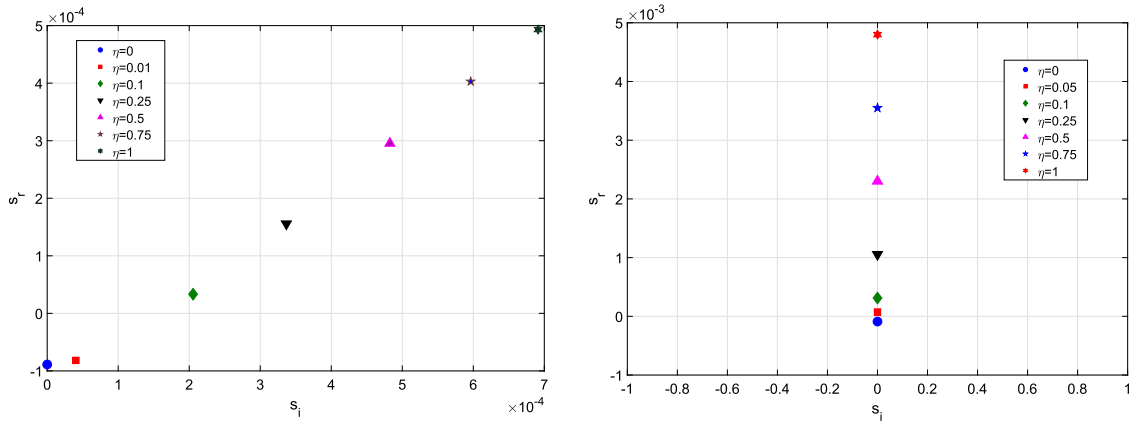

FIG. 2. Variation of the complex growth rate of the (a) streamwise long-wave mode for $k = 0.01$ and $m = 0$ and (b) spanwise long-wave mode for $k = 0$ and $m = 0.01$ with an increase in η in the case of the return flow. The parameters set here is $Bi = 0$, $Bo = 0.1$, $Pr = 7$, $Ma = 10$, $\zeta = 0$, and $Ca = 0.001$. The HTG component of the imposed OTG makes the streamwise long-wave mode an upstream mode, whereas the spanwise long-wave mode remains stationary. An increase in the strength of the HTG, i.e., in η, leads to an increase in the growth rate of both modes. Thus, the HTG has a destabilizing effect on both the streamwise and spanwise long-wave modes.

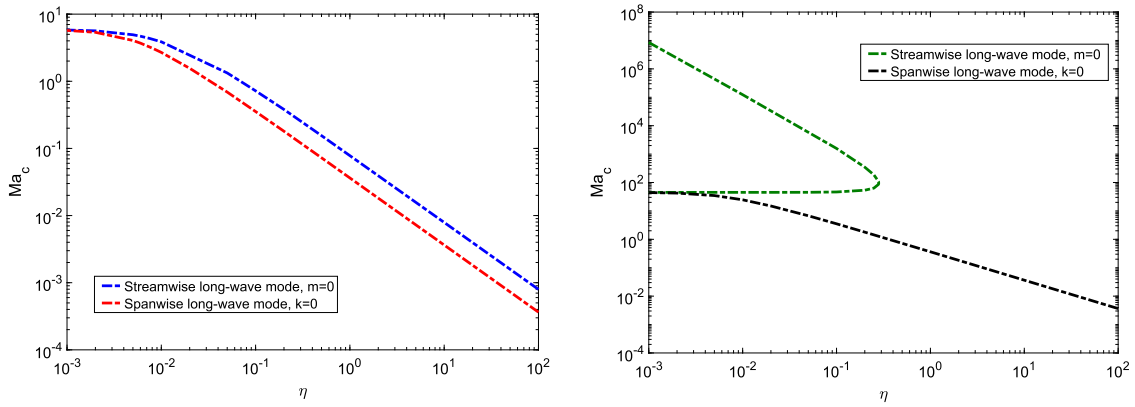

FIG. 3. Variation of the critical Marangoni number Ma_c with η at $Bi = 0$, $Bo = 0.1$, $\zeta = 0$, and $Pr = 7$ for the return flow. (a) $Ca = 0.01$; (b) $Ca = 0.0001$. In both panels, the spanwise mode exhibits scaling $Ma_c \sim 1/\eta$, whereas the streamwise long-wave mode exhibits a similar scaling for $Ca = 0.01$ but forms an island of instability for $Ca = 0.0001$. The figure illustrates that an increasing deformability of the interface, i.e., higher values of Ca, promotes the emergence of the streamwise long-wave mode for larger values of η. The spanwise long-wave mode exists at larger values of η independently of the interface deformability, although an increasing interface deformability equivalent to an increasing Ca lowers the critical Marangoni number Ma_c.

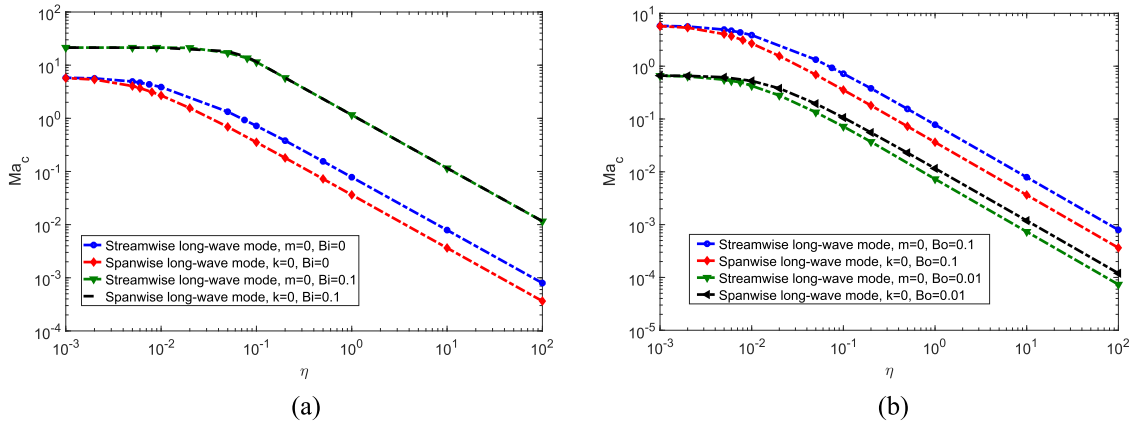

FIG. 4. Variation of the critical Marangoni number Ma_c with η at $Ca = 0.01$, $\zeta = 0$, and $Pr = 7$ for the return flow. (a) An increase in the Biot number Bi stabilizes the spanwise long-wave mode more than the streamwise one. Note that the curve corresponding to the spanwise mode for $k = 0$ and $Bi = 0.1$ coincides with that for the streamwise mode for $m = 0$ and $Bi = 0.1$. (b) A decrease in the Bond number Bo leads to destabilization for both modes, which is more pronounced for the streamwise mode. Thus, the streamwise mode is the dominant mode of instability at a lower Bo. Here $Bi = 0$.

critical Marangoni number Ma_c. An increase in Bi causes a dramatic increase in Ma_c for both long-wave modes. The stabilizing effect of an increase in Bi is stronger on the spanwise long-wave mode and leads to the merging of the curves for the streamwise and spanwise modes with $Bi = 0.1$, as shown in Fig. 4(a). Thus, both streamwise and spanwise long-wave modes represent the dominant modes of instability. A decrease in Bo leads to a decrease in Ma_c for both modes, however, to a greater extent for the streamwise mode as compared to the spanwise mode. This causes the streamwise long-wave mode to become the dominant instability mode for a lower Bond number since it is destabilized at lower Ma_c compared to the spanwise long-wave mode. The spanwise mode, however, is dominant for a higher value of the Bond number. The variation in the Prandtl number Pr, albeit not shown here, has a negligible effect on the critical parameters.

Finally, to understand the effect of slippage at the substrate on the critical parameters, a typical variation of Ma_c with the slip parameter ζ is presented in Fig. 5 for a fixed parameter set and typical values of η. In the case of an imposed purely VTG, i.e., $\eta = 0$, the curves for both long-wave streamwise and spanwise modes naturally coincide due to the isotropy in the x–z plane, and an increase in ζ leads to an increase in Ma_c. For $\eta = 0$, the slip at the substrate can only affect the perturbed state through the boundary conditions at the substrate. However, for a non-zero η, slippage at the substrate also affects the base state as seen in Eqs. (7) and (8), which leads to the symmetry breaking of the streamwise and spanwise long-wave

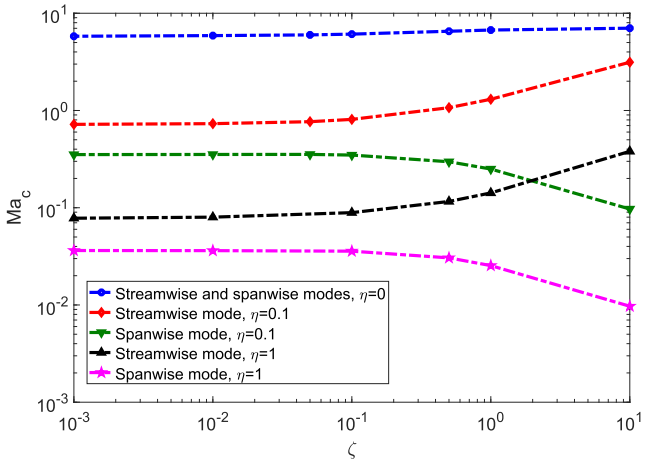

FIG. 5. Variation of the critical Marangoni number Ma_c with the slip parameter ζ for $Bi = 0$, $Bo = 0.1$, $Ca = 0.01$, and $Pr = 7$ in the case of the return flow. In the absence of a HTG, $\eta = 0$, an increasing slippage at the substrate has a stabilizing effect on both modes. In the presence of a HTG, $\eta \neq 0$, slippage stabilizes the streamwise long-wave mode and destabilizes the spanwise long-wave mode.

modes. Figure 5 demonstrates that an increase in the slip coefficient causes an increase in Ma_c in the case of the streamwise long-wave mode and a decrease in Ma_c in the case of the spanwise long-wave mode. Thus, slippage at the substrate has a stabilizing effect on the streamwise long-wave mode and a destabilizing effect on the spanwise long-wave mode.

B. Linear flow

When the effect of the walls along the streamwise direction is neglected, then the thermocapillary flow originating as a consequence of the imposed HTG is a linear flow. The effect of the linear flow on the streamwise and spanwise long-wave modes due to the imposed OTG is shown in Fig. 6. While with an increase in η, the imposed HTG leads to an increase in the growth rate of the streamwise long-wave mode similar to the case of the return flow, for the spanwise long-wave mode, a non-vanishing HTG leads to the emergence of a pair of spanwise modes originating as a result of the splitting of an eigenvalue present for an imposed purely VTG having symmetry in the x–z plane. The lack of a counteracting VTG induced due to the imposed HTG for the present problem leads to the absence of stabilization that was observed by Patne *et al.*,[26] where the system was held at a constant temperature difference across the layer. In addition, the emerging streamwise long-wave mode propagates downstream, which is different from the case of the return flow.

The variation of the critical value of the Marangoni number Ma_c with the relative strength of the HTG η is presented in Fig. 7. If the HTG is weaker compared to the VTG, i.e., $\eta < 1$, then the streamwise long-wave mode determines the stability of the system. In the limit of small η, both modes exhibit an increase in Ma_c with the spanwise mode displaying a larger increase as compared to the streamwise one, making the overall variation of Ma_c with η non-monotonic, as shown in Fig. 7. This differential stabilizing effect with an increase in the HTG at low η makes the streamwise mode to dominate the instability onset there. On the other hand, because of a rapid decrease in Ma_c for the spanwise mode in the domain of $\eta > 0.1$, the situation changes, and in the domain of $\eta > 1$, the spanwise long-wave mode dominates the instability.

As discussed above in the case of the return flow, for higher surface tension, i.e., a lower value of the capillary number, e.g., $Ca = 0.0001$, the streamwise long-wave mode forms an island of long-wave instability presented in Fig. 3(b). However, in the case of the linear flow, both long-wave instability modes transform to become finite-waves, i.e., with finite k_c and m_c, as η increases. Neutral stability curves for a representative value of $\eta = 0.5$ for both streamwise

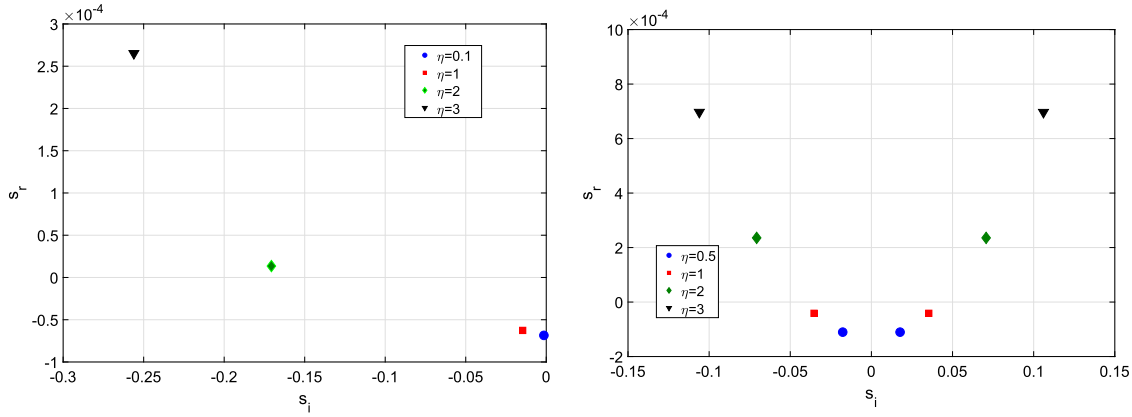

FIG. 6. Variation of the leading eigenvalue with η for $Bi = 0$, $Bo = 0.1$, $Pr = 7$, $Ma = 5$, $\zeta = 0$, and $Ca = 0.001$ in the case of the linear flow for (a) the streamwise long-wave mode with $k = 0.01$ and $m = 0$ and (b) the spanwise long-wave mode with $k = 0$ and $m = 0.01$. An increase in η leads to an increase in the growth rate of both streamwise and spanwise long-wave modes. The streamwise long-wave mode propagates downstream. The spanwise long-wave mode consists of a pair of long-wave modes with the same growth rate and two frequencies with a different sign, i.e., traveling in opposite directions at the same speed.

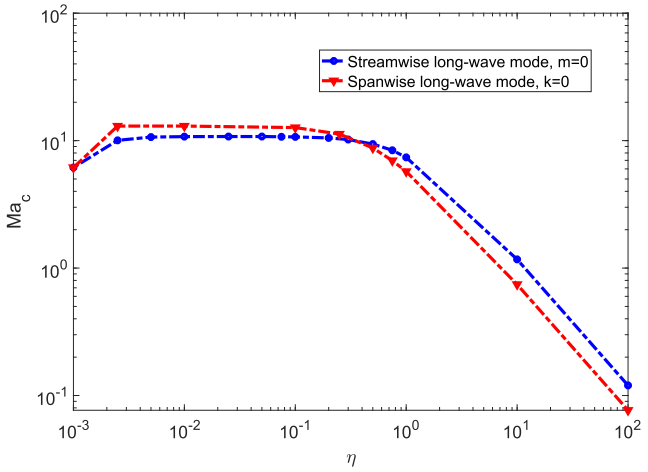

FIG. 7. Variation of the critical Marangoni number Ma_c with η for $Bi = 0$, $Bo = 0.1$, $Ca = 0.01$, $\zeta = 0$, and $Pr = 7$ in the case of the linear flow. If the strength of the HTG is weaker than that of the VTG, i.e., $\eta < 1$, then the streamwise long-wave mode is the dominant mode of instability, while for $\eta > 1$, the spanwise long-wave mode dominates the system stability. Both modes scale as $Ma_c \sim 1/\eta$ for $\eta > 1$. Thus, in contrast to the return flow, for the linear flow, both modes of instability play a major role and compete in determining the stability of the system.

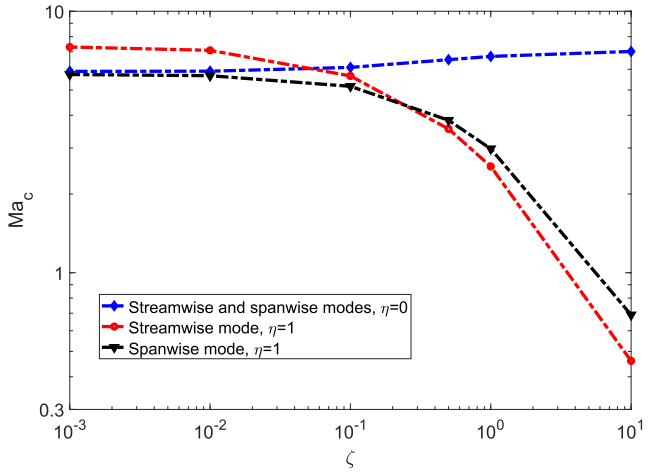

FIG. 9. Variation of the critical Marangoni number Ma_c with the slip parameter ζ at $Bi = 0$, $Bo = 0.1$, $Ca = 0.01$, and $Pr = 7$ for the linear flow. Slippage at the substrate has a small stabilizing effect on both long-wave modes when only the VTG is imposed. However, for a nonzero η, an increase in the slip coefficient has a destabilizing effect on both the long-wave modes in contrast to the return flow, as shown in Fig. 5.

and spanwise modes are displayed in Fig. 8(a). The critical values of the streamwise k_c and spanwise m_c wavenumbers and the critical Marangoni number Ma_c are determined from the minima of the streamwise and spanwise neutral curves similar to those of Fig. 8(a), respectively, for each value of η. The results are then presented in Fig. 8(b). For $\eta < 0.005$, both instability modes are long-waves in nature and also dominant modes. For $0.005 < \eta < 0.5$, the critical Marangoni number is almost constant, while the critical wavenumbers slowly increase with an approximate scaling of $\eta^{0.1}$. For $\eta > 0.5$, the scaling for the critical Marangoni number is $Ma_c \sim 1/\eta$, whereas k_c and m_c each attain a constant value of $O(1)$. The effect of variation of other parameters such as Bi, Bo, and Pr is qualitatively similar to that presented above in the case of the return flow. Thus, in the interest of brevity, those results are not presented here.

Finally, the impact of the slip at the substrate on the critical parameters is shown in Fig. 9. For the return flow, as shown in Fig. 5, an increase in slippage at the substrate has a stabilizing effect on the streamwise long-wave mode and a destabilizing effect on the spanwise long-wave mode provided that the HTG has a nonzero value.

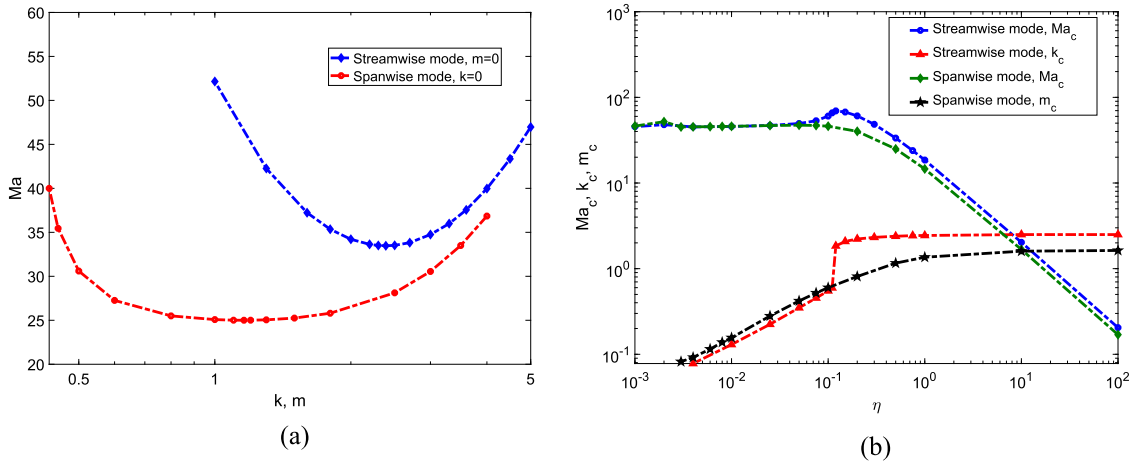

FIG. 8. Instability of the system with $Bi = 0$, $Bo = 0.1$, $\zeta = 0$, $Ca = 0.0001$, and $Pr = 7$ in the case of the linear flow. (a) Neutral stability curves for $\eta = 0.5$ exhibit finite-wave modes illustrating the transition of the long-wave instability to the finite-wave instability. (b) Variation of the critical values of the wavenumbers k_c, m_c and the Marangoni number Ma_c with η. While Ma_c scales as $Ma_c \sim 1/\eta$ for $\eta > 1$, the critical wavenumbers each tend to a constant finite value. The figure illustrates switching from the long-wave streamwise and spanwise modes emerging for higher Ca as in Fig. 7 to the finite-wave modes with an increase in the relative strength of the HTG η.

However, Fig. 9 demonstrates that for a nonzero η, an increase in the slip coefficient leads to a decrease in Ma_c for both the long-wave modes. For the streamwise long-wave mode, a decrease in Ma_c with an increase in ζ is stronger than that in the spanwise long-wave mode, thereby making it the dominant mode of instability. Thus, slippage at the substrate can lead to a qualitative change in the stability map of the system by switching between the dominant modes of instability.

V. LONG-WAVE ASYMPTOTIC ANALYSIS

In this section, the asymptotic analysis is carried out in the long-wave limit with an emphasis on the role of the HTG in the stabilization of the long-wave streamwise instability triggered by the presence of the VTG in the limit of small η. This feature is observed in both the return and linear flows as demonstrated in Figs. 3 and 8(b), respectively. The following analysis is restricted to the nondeformable case, i.e., $Ca = 0$ and $Bo = 0$, and no-slip ($\zeta = 0$) boundary condition at the substrate. The governing equations for the perturbations (10) remain the same, while the boundary conditions at the substrate $y = 0$ become

$$\tilde{v}_x = 0, \quad \tilde{v}_y = 0, \quad \tilde{v}_z = 0, \quad D\tilde{T} = 0. \tag{15a}$$

At the free surface $y = 1$, the assumption of a nondeformable interface ($Ca = 0$) leads to the boundary conditions

$$\tilde{v}_y = 0, \tag{15b}$$

$$D\tilde{v}_x = -ik\,Ma\tilde{T}, \tag{15c}$$

$$D\tilde{T} + Bi\tilde{T} = 0. \tag{15d}$$

The continuity of the normal stress at the free surface is satisfied automatically.

In what follows, we assume two-dimensional streamwise disturbances with $m = 0$. In the governing equations (10) and boundary conditions (11), the streamwise and transverse eigenfunctions of the perturbation velocities are expressed via the streamfunction ψ using the relation

$$\tilde{v}_x(y) = D\psi(y), \quad \tilde{v}_y(y) = -ik\psi(y). \tag{16}$$

As noted above, we assume small values of η, $\eta = \epsilon\hat{\eta}$, so that $\hat{\eta} = O(1)$ and $\epsilon \ll 1$, and apply the following scaling:[39]

$$k = \epsilon\hat{k}, \quad s = \epsilon^2\hat{s}, \quad Bi = \epsilon^4\widehat{Bi}, \quad \psi = \epsilon\hat{\psi} \tag{17}$$

with hat decoration used to denote the scaled values. Equation (17) is then substituted into the governing equations (10) and the boundary conditions (15) modified using Eq. (16). Furthermore, the scaled streamfunction, the growth rate, the temperature, and the Marangoni number are expanded as

$$\hat{\psi} = \psi_0 + \epsilon^2\psi_2 + \epsilon^4\psi_4 + \cdots, \tag{18a}$$

$$\hat{T} = T_0 + \epsilon^2 T_2 + \epsilon^4 T_4 + \cdots, \tag{18b}$$

$$Ma = Ma_0 + \epsilon^2 Ma_2 + \epsilon^4 Ma_4 + \cdots, \tag{18c}$$

$$\hat{s} = s_0 + \epsilon^2 s_2 + \epsilon^4 s_4 + \cdots. \tag{18d}$$

Following elimination of pressure, Eqs. (10) and (11) are rewritten along with Eq. (18) to yield at the zeroth order approximation

$$D^4\psi_0 = 0, \quad D^2 T_0 = 0. \tag{19a}$$

The boundary conditions at $y = 0$ and $y = 1$ become

$$z = 0: \qquad \psi_0 = 0, \quad D\psi_0 = 0, \quad DT_0 = 0, \tag{19b}$$

$$z = 1: \qquad \psi_0 = 0, \quad D^2\psi_0 + ik\,Ma_0\,T_0 = 0, \quad DT_0 = 0, \tag{19c}$$

respectively. Note that Eqs. (19) do not contain the base-state components, and thus, they are valid for both the return and linear flows.

Equations (19) admit the solution for ψ_0 and T_0 in the form

$$T_0 = \alpha_1, \quad \psi_0 = 12\alpha_1\, i\hat{k}\,(1-y)\,y^2, \tag{20}$$

where α_1 is an arbitrary constant, which, for the sake of linear stability analysis, may be set equal to unity without loss of generality.

At $O(\epsilon^2)$, the governing equations for the return and linear flows differ due to the presence of the base-state components. In what follows, we present the solution procedure for the return flow. A similar procedure can also be carried out for the linear flow.

For the return flow, the bulk equations (10) at $O(\epsilon^2)$ read as

$$6\,i\hat{\eta}\hat{k}\,Ma_0\,\psi_0 - \left[8\hat{k}^2\,Pr + 4\,s_0 + i\hat{\eta}\hat{k}\,Ma_0\,y\,(-2+3y)\right]D^2\psi_0 + 4\,PrD^4\psi_2 = 0, \tag{21a}$$

$$-i\hat{k}\,\psi_0 - \frac{1}{4}\left[4\,s_0 + \hat{k}\left(4\hat{k} + i\hat{\eta}\,Ma_0\,y\,(-2+3y)\right)\right]T_0 + \hat{\eta}\,D\psi_0 + D^2 T_2 = 0. \tag{21b}$$

The boundary conditions (15) at $O(\epsilon^2)$ are, respectively,

$$y = 0: \quad \psi_2 = 0, \quad D\psi_2 = 0, \quad DT_2 = 0 \tag{22a}$$

and

$$y = 1: \quad \psi_2 = 0, \quad D^2\psi_2 + ik\,Ma_0\,T_2 = 0, \quad DT_2 = 0. \tag{22b}$$

To obtain the leading-order approximation for the growth rate s_0, Eq. (21b) is integrated with respect to y across the layer $y \in (0, 1)$ and the boundary conditions at $y = 0$ and $y = 1$, Eq. (22), are utilized. The resulting equation is then solved for s_0 to yield

$$s_0 = \frac{1}{48}\hat{k}^2(-48 + Ma_0). \tag{23a}$$

A similar procedure for the linear flow leads to

$$s_0 = \frac{1}{48}\hat{k}\left[\hat{k}(-48 + Ma_0) - 24\,i\hat{\eta}\,Ma_0\right]. \tag{23b}$$

The instability threshold is determined by the growth rate s_r crossing from the negative to the positive value via $s_r = 0$. Therefore, Eq. (23) yields the value of the Marangoni number $Ma_0 = 48$, which is in agreement with that of Pearson[1] and validates the current analysis. Another interesting feature to note is that while the imaginary part of s_0 for the return flow vanishes, it is nonzero for the linear flow. This is a consequence of the velocity fields of the average

base state for both flows. In the case of the return flow, the average base-state velocity vanishes due to the boundary condition (6c); thus, the long-wave disturbances do not propagate in the x-direction at $O(1)$. However, for the linear flow, the average base-state velocity is nonzero and given by $\eta Ma/2$, which represents the travel speed of long-wave disturbances, as obtained from the imaginary part of Eq. (23b).

In the case of the return flow, the solution of Eq. (21) at $O(\epsilon^2)$ satisfying the boundary conditions (22) is

$$\psi_2 = \frac{\hat{k}^2(y-1)y^2\hat{\eta}Ma_0^2}{6720Pr}\left[-19+2y(3+3y-4y^2+3y^3)\right] - \frac{28i\hat{k}(y-1)y}{6720Pr}\left(60Ma_2Pry+2\hat{k}^2Ma_0Pry(-3-2y+3y^2)\right) - \frac{28i\hat{k}(y-1)y}{6720Pr}\left[Ma_0s_0y(-3+y(-2+3y)) + 60Ma_0PryT_2(y=1)\right], \tag{24a}$$

$$T_2 = \frac{1}{240}\left[10i\hat{\eta}\hat{k}Ma_0y^3(-4+3y)+120(2\alpha_2+s_0y^2)\right] + \frac{\hat{k}^2y^2}{2}\left[120+Ma_0y^2(-5+3y)\right], \tag{24b}$$

where α_2 is an integration constant.

At $O(\epsilon^4)$, the energy equation reads as

$$\hat{\eta}^2\hat{k}Ma_0(-1+y)y^2\psi_0+4\hat{k}\psi_2-4is_2T_0-2\hat{\eta}\hat{k}Ma_2yT_0 +3\hat{\eta}\hat{k}Ma_2y^2T_0-4i\hat{k}^2T_2-4is_0T_2-2\hat{\eta}\hat{k}Ma_0yT_2 +3\hat{\eta}\hat{k}Ma_0y^2T_2+4i\hat{\eta}D\psi_2+4iD^2T_4=0. \tag{25}$$

To obtain s_2, the solution of $O(\epsilon^2)$ given by Eq. (21) needs to be substituted into Eq. (25), and the latter is integrated with respect to y across the layer $y \in (0, 1)$ along with the boundary conditions

$$y=0: \quad DT_4=0, \text{ and } \quad y=1: \quad DT_4=-\widehat{Bi}T_0. \tag{26}$$

As a result, we obtain in the case of the return flow

$$s_2 = -\widehat{Bi} - \frac{1}{1680Pr}\hat{k}^2\Big(6912\hat{\eta}^2Pr+7(16\hat{k}^2-5Ma_2)Pr +168i\hat{\eta}\hat{k}(4+13Pr)\Big). \tag{27a}$$

A similar procedure followed for the linear flow yields

$$s_2 = -\widehat{Bi} - \frac{72\hat{\eta}^2\hat{k}^2}{5} - \frac{\hat{k}^4}{15} + \frac{\hat{k}^2Ma_2}{48} - \frac{i\hat{\eta}\hat{k}}{70Pr} \times\left[35Ma_2Pr+\hat{k}^2(40+426Pr)\right]. \tag{27b}$$

It must be noted that the real part of s_2 contributes to the growth of the perturbations when the HTG appears via $\hat{\eta}$.

As obtained from Eq. (27), the real part of s_2, $s_{2r} \equiv \Re(s_2)$, reads as

$$s_{2r} = -\widehat{Bi} - \frac{\hat{k}^2}{1680}\left[6912i\hat{\eta}^2+7(16\hat{k}^2-5Ma_2)\right], \quad \text{for the return flow,} \tag{28a}$$

$$s_{2r} = -\widehat{Bi} - \frac{72\hat{\eta}^2\hat{k}^2}{5} - \frac{\hat{k}^4}{15} + \frac{\hat{k}^2Ma_2}{48}, \quad \text{for the linear flow.} \tag{28b}$$

To enable long-wave instability, i.e., $s_{2r} > 0$ given by Eq. (28) along with $s_{0r} = 0$, around $\tilde{k} = 0$, Ma_2 needs to be positive; then, $k = 0$ is the critical wavenumber and $Ma_0 + \epsilon^2 Ma_2$ is the critical Marangoni number Ma_c up to $O(\epsilon^4)$. Therefore, along the neutral curve, $s_{2r} = 0$ and

$$Ma_2 = \frac{6912\hat{\eta}^2}{5}, \quad \text{for the return flow,} \tag{29a}$$

$$Ma_2 = \frac{3456\hat{\eta}^2}{5}, \quad \text{for the linear flow.} \tag{29b}$$

To facilitate a comparison with the GLSA, we unscale Eq. (29) to obtain the critical Marangoni number for the long-wave mode

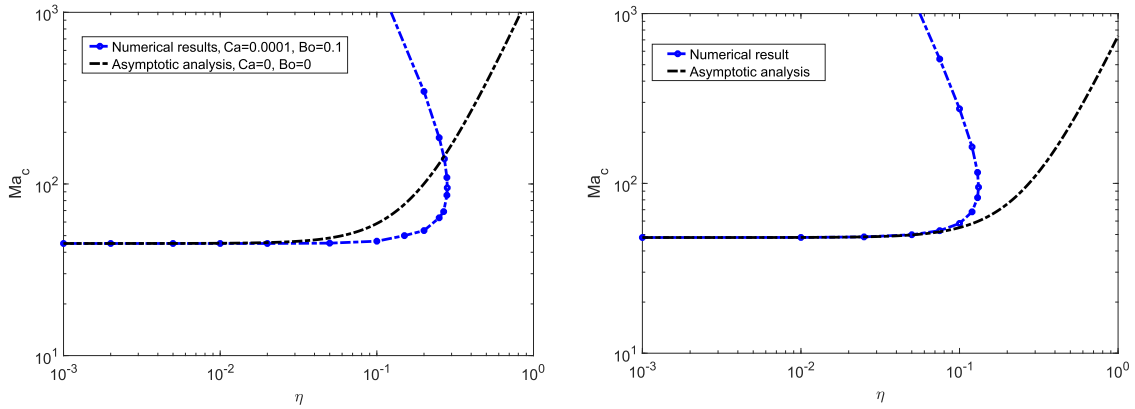

(a) (b)

FIG. 10. Variation of Ma_c with the relative strength of the horizontal temperature gradient η for $Bi = 0$, $Pr = 7$, and $\zeta = 0$ in the case of the streamwise long-wave mode. In both panels, the results of the asymptotic analysis are for $Ca = 0$, $Bo = 0$, whereas the numerical ones are for (a) the return flow with $Ca = 0.0001$, $Bo = 0.1$ and (b) the linear flow with $Ca = 0$, $Bo = 0$. In both panels, the asymptotic and numerical results are in excellent agreement for at least $\eta < 0.06$. Both analyses reveal a strong stabilizing effect of the HTG on the streamwise long-wave mode.

with $Bi = 0$ in the form

$$Ma_c = 48 + \frac{6912\eta^2}{5}, \quad \text{for the return flow} \tag{30a}$$

$$Ma_c = 48 + \frac{3456\eta^2}{5}, \quad \text{for the linear flow.} \tag{30b}$$

It follows from Eq. (30) that with an increase in η, the critical Marangoni number increases, and thus, the presence of a HTG has a stabilizing effect.

The results obtained here based on the asymptotic analysis for the long-wave mode are now compared with those obtained using the pseudo-spectral method for both the return and linear flows in Fig. 10. Interestingly, for the return flow, the asymptotic results are in excellent agreement with the numerical ones obtained for the deformable interface with $Ca = 0.0001$ and $Bo = 0.1$. Thus, as follows from Fig. 10(a), the present asymptotic analysis can be valid for the case of the deformable interface for $\eta < 0.06$. The same excellent agreement is observed in panel (b) for the linear flow, and in the case presented there, it extends up to $\eta = 0.09$. The agreement between the results arising from the numerical and asymptotic analyses can be further improved by considering higher-order corrections to the growth rate, and so for the value of the critical Marangoni number.

VI. SUMMARY

The present paper investigates the stability of a horizontal liquid layer deposited on the substrate with a possible slippage and subjected to an oblique temperature gradient (OTG) with a prescribed constant normal temperature gradient at the substrate. The major differences between the present study and the study of Patne *et al.*[26] are highlighted in Table I. For the return flow, the spanwise mode remains the dominant mode of instability for arbitrary variations in the problem parameters except those in the Bond number Bo. The streamwise long-wave mode is stabilized by the imposed HTG at low Ca, whereas at high Ca, the HTG fails to stabilize the streamwise mode.

In the case of the return flow, the basal slip has a stabilizing effect on the streamwise mode, while the spanwise mode is destabilized in the presence of the HTG. In the absence of the HTG, $\eta = 0$, an increase in the basal slip leads to a slight stabilization of both modes. Thus, the presence of the HTG also influences the effect of the basal slip on the stability. It is notable that in the case of the return flow with an imposed purely HTG, spanwise or streamwise long-wave instability modes are absent.[10] The present analysis shows that as a result of an interaction between the imposed VTG and HTG components, the return flow exhibits both types of instability modes, but these modes dominate the instability onset, even when the HTG is much stronger than the VTG, i.e., in the case of higher values of η. This implies that the presence of a VTG, however small, in a liquid layer may cause the presence of the long-wave modes, thereby imparting a drastic change in the stability features of the liquid layer.

In the case of the linear flow, similar to the return flow, the emergence of the streamwise mode at high η strongly depends on the deformability of the free surface. The streamwise mode determines the stability onset when the VTG is dominant, whereas the spanwise mode determines the stability onset when the HTG is dominant. At low Ca, the linear flow loses stability to finite-wave streamwise and spanwise modes. The basal slip leads to the destabilization of both streamwise and spanwise modes for a nonzero HTG, which may feature a change in the dominant instability mode. In the absence of the HTG, the basal slip leads to the stabilization of both the streamwise and spanwise modes. The asymptotic analysis carried out in the case of the streamwise mode and the nondeformable interface in the limiting case of small η shows an excellent agreement with the results of numerical computations for $\eta < 0.06$.

The present analysis demonstrates that in practical applications such as additive manufacturing, liquid layers subjected to an OTG with a significant basal slip may exhibit qualitatively different types of instabilities compared to those developing when either a purely HTG or a purely VTG is acting on the system. From the point of view of applications, it would be of paramount importance to reveal whether a liquid layer subjected to an OTG preserves its contiguity or ruptures, and, in the latter case, whether this rupture can be prevented or controlled. Therefore, weakly nonlinear and fully nonlinear analyses of the system dynamics would be the next step in the study of the present problem. The present paper could also be extended to the case of self-rewetting liquids whose surface tension is represented by a nonlinear function of the temperature.

TABLE I. Summary of the differences between the system in the study of Patne *et al.*[26] and in the present paper. As indicated by the first row of the table, the difference in the stability properties between the two systems arises primarily due to the thermal boundary condition at the substrate. The present paper is relevant to the case of a poorly conducting substrate as compared to the liquid, whereas the results in the study of Patne *et al.*[26] are applicable to a highly conductive substrate as compared to the liquid. Here, LW stands for long-wave and the interaction mode refers to the thermocapillary instability mode arising due to the interaction[26] between the imposed HTG and VTG.

System features	This paper	Patne *et al.*[26]
Temperature BC at the substrate	$\partial_{y^*} T^* = -\beta^*$	$T^* = T_0^* - \eta^* x^*$
Velocity BC at the substrate	With and with no slip	No slip
Induced VTG by the HTG	Absent	Present
Types of flows	Linear and return flows	Linear flow
Dominant mode at high η	Spanwise LW mode	Interaction mode

ACKNOWLEDGMENTS

This research was supported by the Israel Science Foundation (ISF) under Grant No. 356/18. R.P. was partially supported by the Technion Funds Postdoctoral Fellowship. Y.A. was partially supported by the Millstone/St. Louis Chair in Civil and Environmental Engineering. A.O. was partially supported by the David T. Siegel Chair in Fluid Mechanics.

DATA AVAILABILITY

The data that support the findings of this study are available within this article.

REFERENCES

[1] J. R. A. Pearson, "On convection cells induced by surface tension," J. Fluid Mech. **4**, 489–500 (1958).
[2] L. E. Scriven and C. V. Sternling, "On cellular convection driven by surface-tension gradients: Effects of mean surface tension and surface viscosity," J. Fluid Mech. **19**, 321–340 (1964).
[3] K. A. Smith, "On convective instability induced by surface-tension gradients," J. Fluid Mech. **24**, 401–414 (1966).
[4] S. H. Davis and G. M. Homsy, "Energy stability theory for free-surface problems: Buoyancy-thermocapillary layers," J. Fluid Mech. **98**, 527–553 (1980).
[5] C. Pérez-Garcia and G. Carneiro, "Linear stability analysis of Bénard–Marangoni convection in fluids with a deformable free surface," Phys. Fluids A **3**, 292–298 (1991).
[6] A. Karbalaei, R. Kumar, and H.-J. Cho, "Thermocapillarity in microfluidics—A review," Micromachines **7**, 13 (2016).
[7] K. N. Kowal, S. H. Davis, and P. W. Voorhees, "Thermocapillary instabilities in a horizontal liquid layer under partial basal slip," J. Fluid Mech. **855**, 839–859 (2018).
[8] M. Lappa, *Thermal Convection: Patterns, Evolution and Stability* (Wiley, 2010).
[9] S. F. Kistler and P. M. Schweizer, *Liquid Film Coating: Scientific Principles and Their Technological Implications* (Springer, Dordrecht, 1997).
[10] M. K. Smith and S. H. Davis, "Instabilities of dynamic thermocapillary liquid layers. Part 1. Convective instabilities," J. Fluid Mech. **132**, 119–144 (1983).
[11] M. K. Smith and S. H. Davis, "Instabilities of dynamic thermocapillary liquid layers. Part 2. Surface-wave instabilities," J. Fluid Mech. **132**, 145–162 (1983).
[12] K.-X. Hu, M. He, and Q.-S. Chen, "Instability of thermocapillary liquid layers for Oldroyd-B fluid," Phys. Fluids **28**, 033105 (2016).
[13] K.-X. Hu, M. He, Q.-S. Chen, and R. Liu, "Linear stability of thermocapillary liquid layers of a shear-thinning fluid," Phys. Fluids **29**, 073101 (2017).
[14] K.-X. Hu, C.-Y. Yan, and Q.-S. Chen, "Instability of thermocapillary–buoyancy convection in droplet migration," Phys. Fluids **31**, 122101 (2019).
[15] D. Schwabe, U. Möller, J. Schneider, and A. Scharmann, "Instabilities of shallow dynamic thermocapillary liquid layers," Phys. Fluids A **4**, 2368–2381 (1992).
[16] R. J. Riley and G. P. Neitzel, "Instability of thermocapillary–buoyancy convection in shallow layers. Part 1. Characterization of steady and oscillatory instabilities," J. Fluid Mech. **359**, 143–164 (1998).
[17] S. Benz, P. Hintz, R. J. Riley, and G. P. Neitzel, "Instability of thermocapillary–buoyancy convection in shallow layers. Part 2. Suppression of hydrothermal waves," J. Fluid Mech. **359**, 165–180 (1998).
[18] M. F. Schatz and G. P. Neitzel, "Experiments on thermocapillary instabilities," Annu. Rev. Fluid Mech. **33**, 93–127 (2001).
[19] N. A. Ospennikov and D. Schwabe, "Thermocapillary flow without return flow–linear flow," Exp. Fluids **36**, 938–945 (2004).
[20] D. Schwabe, "Convective instabilities in complex systems with partly free surface," J. Phys.: Conf. Ser. **64**, 012001 (2007).
[21] S. H. Davis, "Thermocapillary instabilities," Annu. Rev. Fluid Mech. **19**, 403–435 (1987).
[22] A. A. Nepomnyashchy, I. B. Simanovskii, and L. M. Braverman, "Stability of thermocapillary flows with inclined temperature gradient," J. Fluid Mech. **442**, 141–155 (2001).
[23] A. A. Nepomnyashchy and I. B. Simanovskii, "Dynamics of ultra-thin two-layer films under the action of inclined temperature gradients," J. Fluid Mech. **631**, 165–197 (2009).
[24] A. A. Nepomnyashchy and I. B. Simanovskii, "Marangoni waves in a two-layer film under the action of an inclined temperature gradient," Phys. Fluids **26**, 082102 (2014).
[25] I. B. Simanovskii, A. Viviani, F. Dubois, and J.-C. Legros, "The influence of the horizontal component of the temperature gradient on nonlinear convective oscillations in two-layer systems," Phys. Fluids **24**, 102108 (2012).
[26] R. Patne, Y. Agnon, and A. Oron, "Thermocapillary instabilities in a liquid layer subjected to an oblique temperature gradient," J. Fluid Mech. (to be published).
[27] R. Sarma and P. K. Mondal, "Marangoni instability in a heated viscoelastic liquid film: Long-wave versus short-wave perturbations," Phys. Rev. E **100**, 013103 (2019).
[28] A. Oron and P. Rosenau, "On a nonlinear thermocapillary effect in thin liquid layers," J. Fluid Mech. **273**, 361–374 (1994).
[29] W. Batson, Y. Agnon, and A. Oron, "Thermocapillary modulation of self-rewetting films," J. Fluid Mech. **819**, 562–591 (2017).
[30] R. Sarma and P. K. Mondal, "Marangoni instability in a thin film heated from below: Effect of nonmonotonic dependence of surface tension on temperature," Phys. Rev. E **97**, 043105 (2018).
[31] H. Zuo, F. Javadpour, S. Deng, and H. Li, "Liquid slippage on rough hydrophobic surfaces with and without entrapped bubbles," Phys. Fluids **32**, 082003 (2020).
[32] P. J. Schmid and D. S. Henningson, *Stability and Transition in Shear Flows* (Springer, New York, 2001).
[33] L. N. Trefethen, *Spectral Methods in MATLAB* (SIAM, Philadelphia, 2000).
[34] R. Patne, Y. Agnon, and A. Oron, "Marangoni instability in the linear Jeffreys fluid with a deformable surface," Phys. Rev. Fluids **5**, 084005 (2020).
[35] A. B. Ezersky, A. Garcimartin, H. L. Mancini, and C. Pérez-Garcia, "Spatiotemporal structure of hydrothermal waves in Marangoni convection," Phys. Rev. E **48**, 4414 (1993).
[36] M. Li, S. Xu, and E. Kumacheva, "Convection in polymeric fluids subjected to vertical temperature gradients," Macromolecules **33**, 4972–4978 (2000).
[37] A. I. Mizev and D. Schwabe, "Convective instabilities in liquid layers with free upper surface under the action of an inclined temperature gradient," Phys. Fluids **21**, 112102 (2009).
[38] S. J. Bolanos and B. Vernescu, "Derivation of the Navier slip and slip length for viscous flows over a rough boundary," Phys. Fluids **29**, 057103 (2017).
[39] A. Oron and A. A. Nepomnyashchy, "Long-wavelength thermocapillary instability with the Soret effect," Phys. Rev. E **69**, 016313 (2004).